CHAPTER 4

Results and Discussion

4.1 Fourier Transform-Infrared Spectroscopy (FT-IR)

Infrared spectroscopy is the study of the interactions between infrared radiation and compounds. The IR spectrum generally covers the region from 400-4000cm $^{-1}$. This is because all organic molecules, and some inorganic ions, absorb in this region. The range 400-4000cm $^{-1}$ can be roughly divided into three important areas.

(a) Functional group region ranges from 4000-1300cm $^{-1}$. This region is particularly important for identifying the stretch mode of functional groups such as O-H, N-H and C=O.

(b) Fingerprint region ranges approximately from 1430 to 910 cm^{-1}. The absorption pattern in this part of spectrum is usually complex due to both stretching and bending modes. This region can be used to identify an organic compound, as each organic compound has its own unique pattern.

(c) Low energy region ranges from 909 to 667 cm^{-1}

FT-IR was carried out on samples, which were calcined for five hours at 400°C and 800°C. The samples, which were calcined at 800°C, were subjected to further heating for nine hours at the same temperature and FT-IR was also carried on these samples. Figures 4.1- 4.12 show the IR spectra of the calcined samples. The FT-IR spectra will indicate the presence of organic molecules or absence of organic molecules in the calcined samples. If the material is relatively pure, peaks attributable to the nitrates, tartrates and hydroxides (except water) will not be observed.

In this work we have used $LiOH.H_2O$, $Co(NO_3)_2.6H_2O$, $Ni(NO_3)_2.6H_2O$, tartaric acid and ammonia solution (to control the pH). It is expected that after heating for the chosen temperatures of the associated periods, peaks due to hydroxide, nitrates and tartrates would disappear. FT-IR spectroscopy was carried out to confirm this.

Table 4.1 gives the absorption bands of F samples treated at different temperatures.

T°C	400(5hrs)	800(5hrs)	800(14hrs)
Absorption	3409.2	3436.07	3436.72
		1711.03	
Band cm^{-1}	1632.55	1613.58	1612.41
	1484.74	1494.34	1112.2
	1440.15	1442	659.85
	1129.74	1118.85	
	868.81	871.11	
	661.45		
	638.39		
	565.55	570.86	589.49

The broad band at approximately 3400 cm^{-1} can be identified as O-H stretching modes, which could be due to presence of hydroxide, hydroxyl in the metal tartrate or water. The other peaks seen in the region of 1400 to 1600 cm^{-1} and 1000 to 1300 cm^{-1} are characteristic of vibration modes of C= O group and C-O group. These peaks arise, from vibrations related to tartrate ligands. Hydroxy tartrate groups which are insoluble in water may also be present in the region of 1400 to 1600 cm^{-1}. Characteristic vibrations of hydroxy tartrate groups are difficult to resolve due to

strong overlap of tartrate ligands in this region (Chang et al, 1998). Peaks present at approximately 861 cm^{-1} and 661 cm^{-1} could be assigned to OCO group (Zishan et al, 2000), which may be due to carbonates. It was reported in (Zhecheva and Stoyanova, 1993), that in $LiMO_2$, the vibrations LiO_2 and MO_2 layers are separated. The MO_6 vibrations are observed in the region of 400-700 cm^{-1} and LiO_6 vibrations are in the region of 200 - 400 cm^{-1}.

From the above analyses, it can be suggested that the following reactions could have taken place. The impurities present in F400 are mainly composed of lithium tartrate. When temperature was raised to 800°C, most of the tartrates were decomposed and lithium carbonate, lithium oxide, cobalt oxide and lithium cobalt oxide was formed. On prolong heating at 800°C most of the lithium carbonate, lithium oxide and nickel oxide had reacted to form F.

The reaction may have proceeded according to the following equations :

$$2LiOH.H_2O + (HOCHCOOH)_2 \longrightarrow Li_2(HOCHCOO)_2 + 4H_2O$$

On heating

$$Li_2(HOCHOO)_2 + 5/2O_2 \longrightarrow Li_2CO_3 + 2H_2O + 3CO_2$$

$$Li_2CO_3 \longrightarrow Li_2O + CO_2$$

$$Co(NO_3)_2.6H_2O \longrightarrow Co(NO_3)_2 + 6H_2O$$

$$Co(NO_3)_2 \longrightarrow CoO + 2NO_2 + 1/2O_2$$

$$Li_2O + 2CoO + 1/2O_2 \longrightarrow 2LiCoO_2$$

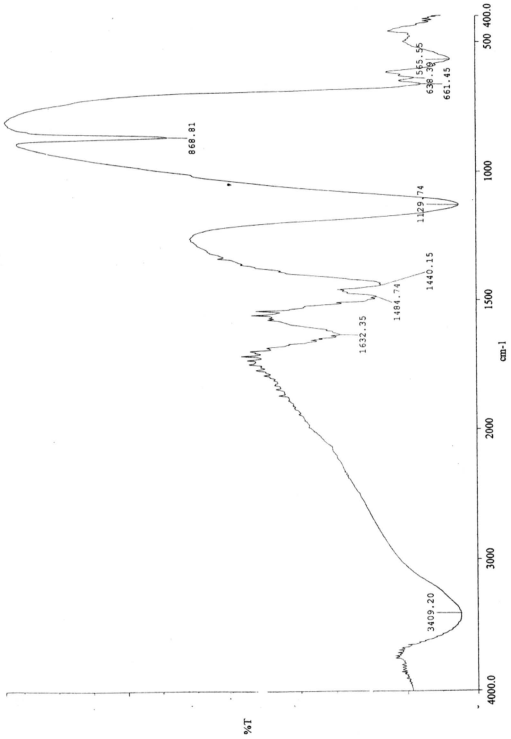

Figure 4.1 : IR spectrum for sample F400 (5hours)

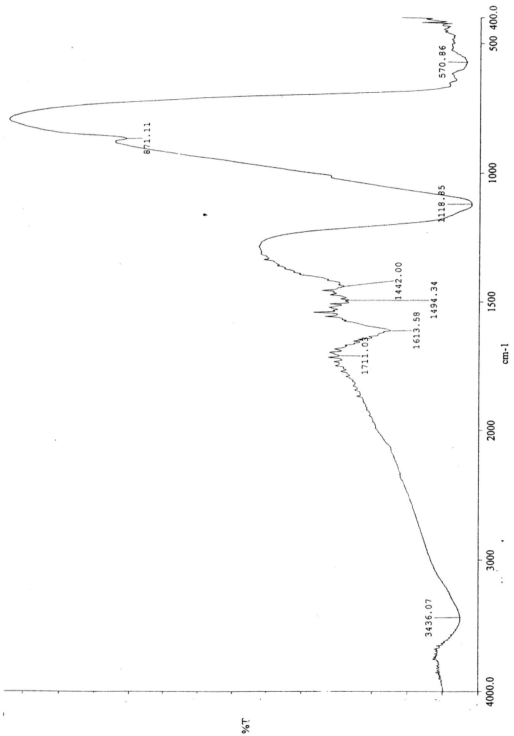

Figure 4.2 : IR spectrum for sample F800 (5 hours)

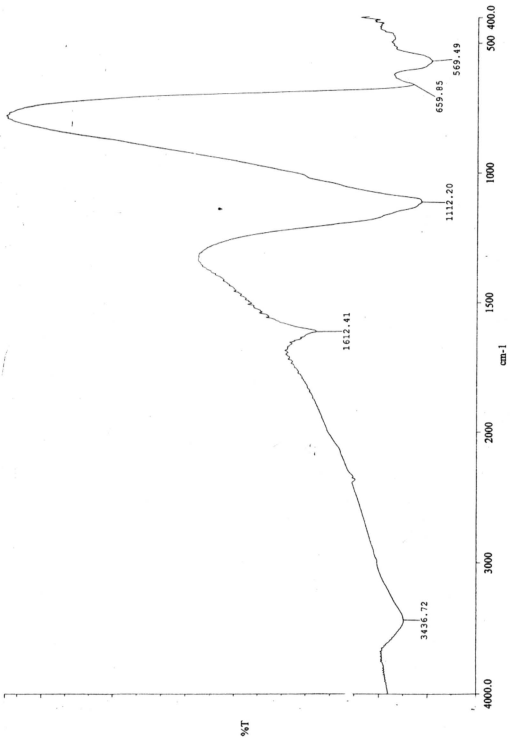

Figure 4.3 : IR spectrum for sample F800 (14 hours)

From the above observations, it can be deduced that the impurities present can be reduced on prolong heating at higher temperature. This may not be in agreement with Prabaharan et al (1998).

Table 4.2 gives the absorption bands of E samples treated at different temperature.

T°C	400(5hrs)	800(5hrs)	800(14hrs)
Absorption Band cm^{-1}	3417.67		
	1494.71		
	1434.77		
	1087.81		
	865.53	864.05	
	497.76	461.03	463.98

E800 (14hrs) has only one peak present at 463.98 cm^{-1}, which is due to Li- O (Zishan et al, 2000). The absence of O-H, C = O and C - O peaks in E800 (14hrs) suggest a pure $LiNiO_2$ is formed. The equations below describes the formation of E.

$$2LiOH.H_2O + (HOCHCOOH)_2 \longrightarrow Li_2(HOCHOO)_2 + 4\,H_2O$$

On heating

$$Li_2(HOCHCOO)_2 + 5/2O_2 \longrightarrow Li_2CO_3 + 2H_2O + 3CO_2$$

$$LiCO_3 \longrightarrow Li_2O + CO_2$$

$$Ni(NO_3)2.6H_2O \longrightarrow Ni(NO_3)_2 + 6H_20$$

$$Ni(NO_3)_2 \longrightarrow NiO + 2NO_2 + 1/2O_2$$

$$Li_2O + 2NiO + 1/2O_2 \longrightarrow 2LiNiO_2$$

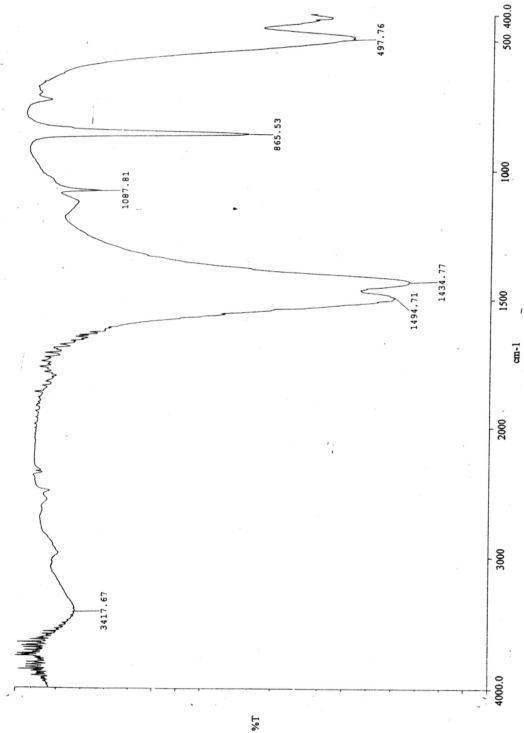

Figure 4.4 : IR spectrum for sample E 400 (5hours)

Figure 4.4 : IR spectrum for sample E 400 (5hours)

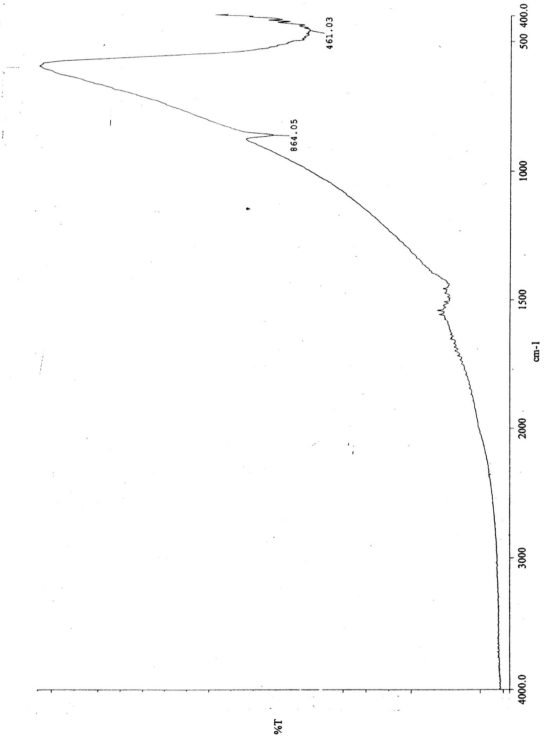

Figure 4.5 : IR spectrum for sample E800 (5hours)

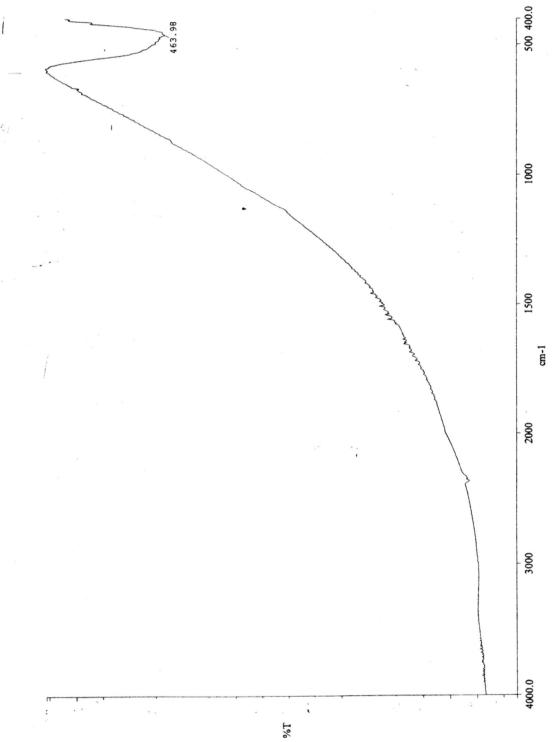

Figure 4.6 : IR spectrum for sample E800 (14hours)

Table 4.3 gives the absorption bands of A samples heated at different temperatures

T°C	400(5hrs)	800(5hrs)	800(14hrs)
Absorption	3421.46	3428.31	
Band cm^{-1}	1633.87	1633.45	1613.48
	1486.37	1494.43	
	1434.75	1434.59	
	1131.03	1129.54	1115.6
	867.59	871.01	
	636.41		604.04
	510.02	463.73	498.17

It was noticed that O-H band, C=O peak and C-O peak was present for calcined temperature of 400°C and 800°C for 5 hours. This indicates impurities of tartrates and carbonates are still present. However, the O-H band was absent in sample, which was heated for fourteen hours at 800°C. This shows absence of tartrates.

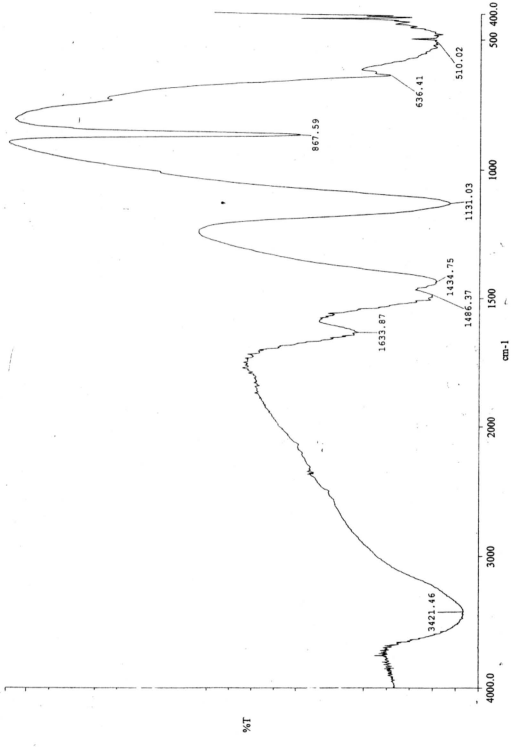

Figure 4.7 : IR spectrum for sample A400 (5hours)

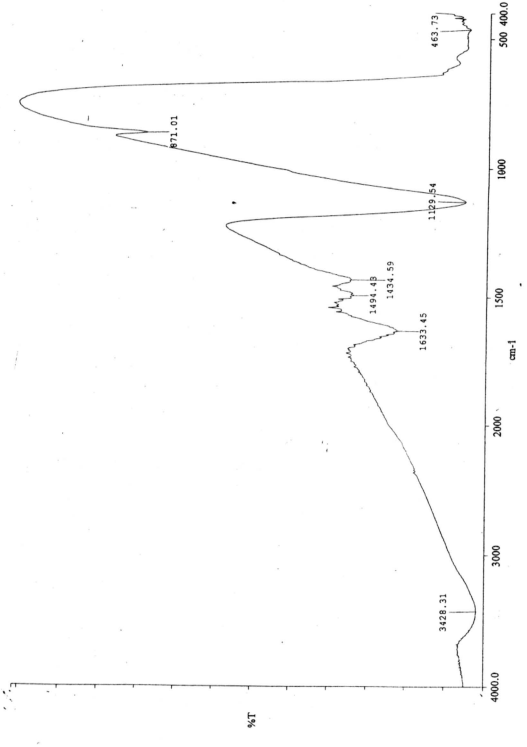

Figure 4.8 : IR spectrum for sample A800 (5hours)

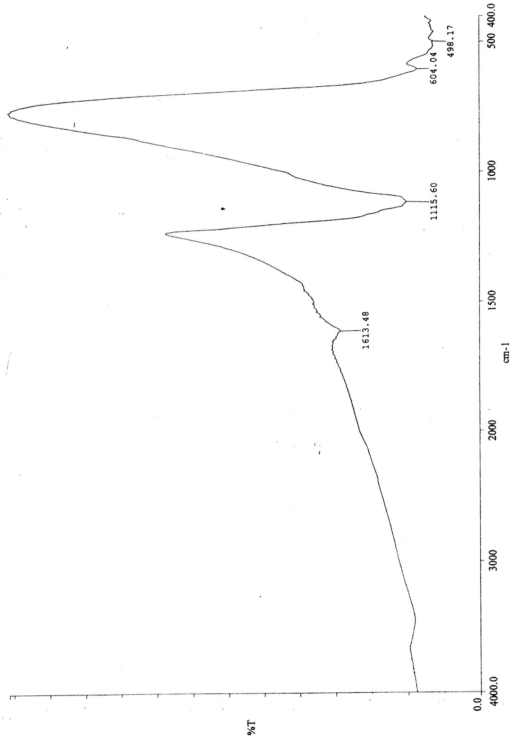

Figure 4.9 : IR spectrum for sample A800 (14hours)

Table 4.4 gives the absorption bands of C sample heated at different temperature

T°C	400(5hrs)	800(5hrs)	800(14hrs)
Absorption	3430.04		
Band cm^{-1}	1806.37		
		1637.87	1650.66
	1501.15	1490.06	
	1433.8	1434.64	
	1130.07	1129.3	1129.44
	866.4	867.86	868.2
	740.63		
	637.88		

The O-H band was present in C400 but was absent when sample was heated at higher temperatures. Compared to sample A, most of the tartrates have decomposed after sample C was heated at 800°C for 5 hours. However, the OCO group was present in all three samples of C, indicating the presence of a carbonate.

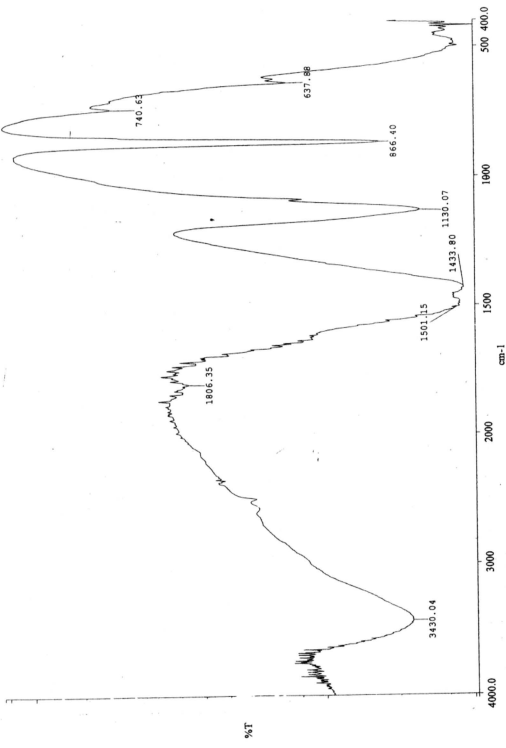

Figure 4.10 : IR spectrum for sample C400 (5hours)

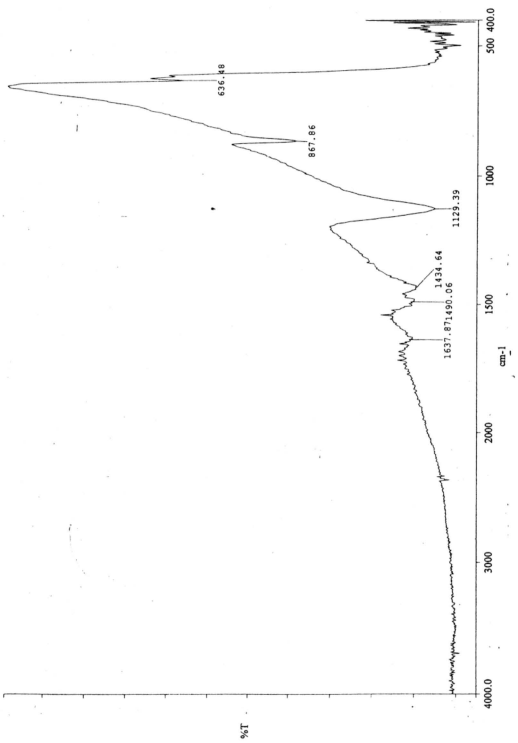

Figure 4.11 : IR spectrum for sample C800 (5hours)

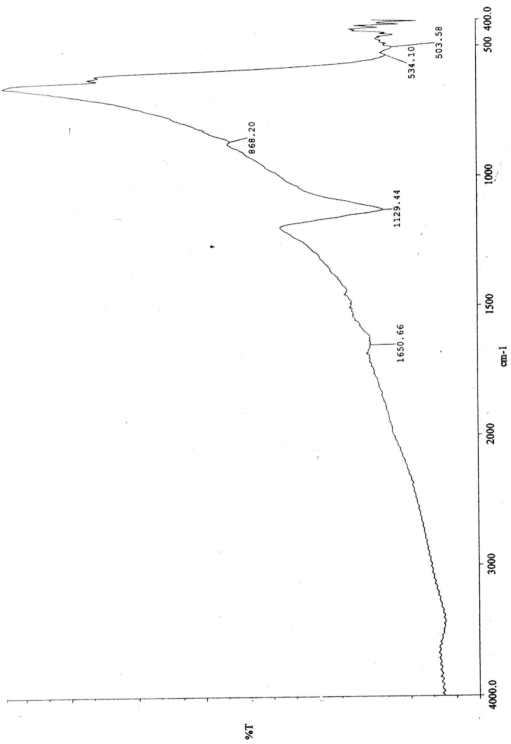

Figure 4.12 : IR spectrum for sample C800 (14hours)

4.2 X-Ray Diffraction (XRD)

XRD can complement FT-IR in structural analysis. FT-IR by itself is not sufficient to provide detailed structural information.

X-ray diffraction was used to identify the crystalline phase of samples A, C, E and F. Figures 4.13 - 4.20 show the XRD pattern for the gel-derived materials calcined at temperature of 400°C and 800°C for five hours, where the molar ratio of tartaric acid to metal ions was 1.0. It was observed, that at higher calcination temperature, there is an increase in peak intensities accompanied by sharpness of peak. This might be attributed to the increase in crystallinity, which may occur from growth of grain size, ordering of local structure, and/or release of lattice strain (Prabaharan et al, 1998; Oh et al, 1997).

For sample F800 which is shown in figure 4.14, peaks at 2θ = 13.4°, 18.8°, 37.2°, 39.0°, 45.2°, 59.5°,65.3° and 66.2°. The main peaks agreed with JCPDS data and result from other researches (Amin et al, 2000; Oh et al, 1997; Tao et al, 1999)to indicate sample is $LiCoO_2$. The small peak observed at 13.5° could be due to small amount of impurities. This observation is in agreement with FT-IR spectra. No peaks were observed for F400 (fig.4.13), which indicating the sample is amorphous. It can be concluded that crystalline $LiCoO_2$ does not form at 400°C.

The XRD pattern for sample E800 is shown in figure 4.16. The peaks at 18.5°,36.2°,37.8°,44.0°,56.2° and 64.0° are in agreement with JCPDS data and results form other researches (Molenda et al, 1999; Zhecheva and Stoyanova, 1993; Chang

et al, 1998). This indicates a relatively pure $LiNiO_2$ can be synthesized at temperature range of 800°C. XRD pattern for E400 shows absence of some main peaks at 18.6° and 64.0°. It was noticed that XRD pattern of E400(fig.4.15) was different to that obtained by Chang et al (1998). This could be due to different preparation method. Chang and fellow researchers used the particulate so-gel method. It is obvious form XRD and IR for E400 there are impurities present which are most likely due to lithium tartrates, lithium carbonates, lithium oxide and nickel oxide.

For sample A800 (fig.4.18), the XRD pattern, show peaks observed at 18.5°,42.2°,42.7°,43.8° and 44.5°. It can be deduced that in order to from pure crystalline $LiCo_{0.4}Ni_{0.6}O_2$ calcination temperature higher than 800°C has to be used. Sample A400 (fig.4.17) was amorphous, since only very small peaks were present.

The XRD pattern of C800 shown in figure 4.20, was compared to that prepared by Zhecheva and Stoyanova (1993) . Zhecheva and Stoyanova (1993) prepared samples by first heating at 300 °C, until the complete evolution of the nitrogen oxides, then homogenized, pelleted and heated at 600°C for 6 hours in air. It was ground again, pelleted and heated at 850°C in air for 30 hours. It can be concluded that to obtain a highly crystalline $LiCo_{0.2}Ni_{0.8}O_2$ will require higher temperature and prolonged heating. Sample C400 (fig.4.19) had extra peaks compared to C800, which was probably due to impurities.

It can be concluded from XRD and IR studies, that sample E, which was calcined for 14 hours at 800°C was the highly crystalline and pure $LiNiO_2$.

et al, 1998). This indicates a relatively pure $LiNiO_2$ can be synthesized at temperature range of 800°C. XRD pattern for E400 shows absence of some main peaks at 18.6° and 64.0°. It was noticed that XRD pattern of E400(fig.4.15) was different to that obtained by Chang et al (1998). This could be due to different preparation method. Chang and fellow researchers used the particulate so-gel method. It is obvious form XRD and IR for E400 there are impurities present which are most likely due to lithium tartrates, lithium carbonates, lithium oxide and nickel oxide.

For sample A800 (fig.4.18), the XRD pattern, show peaks observed at 18.5°,42.2°,42.7°,43.8° and 44.5°. It can be deduced that in order to from pure crystalline $LiCo_{0.4}Ni_{0.6}O_2$ calcination temperature higher than 800°C has to be used. Sample A400 (fig.4.17) was amorphous, since only very small peaks were present.

The XRD pattern of C800 shown in figure 4.20, was compared to that prepared by Zhecheva and Stoyanova (1993) . Zhecheva and Stoyanova (1993) prepared samples by first heating at 300 °C, until the complete evolution of the nitrogen oxides, then homogenized, pelleted and heated at 600°C for 6 hours in air. It was ground again, pelleted and heated at 850°C in air for 30 hours. It can be concluded that to obtain a highly crystalline $LiCo_{0.2}Ni_{0.8}O_2$ will require higher temperature and prolonged heating. Sample C400 (fig.4.19) had extra peaks compared to C800, which was probably due to impurities.

It can be concluded from XRD and IR studies, that sample E, which was calcined for 14 hours at 800°C was the highly crystalline and pure $LiNiO_2$.

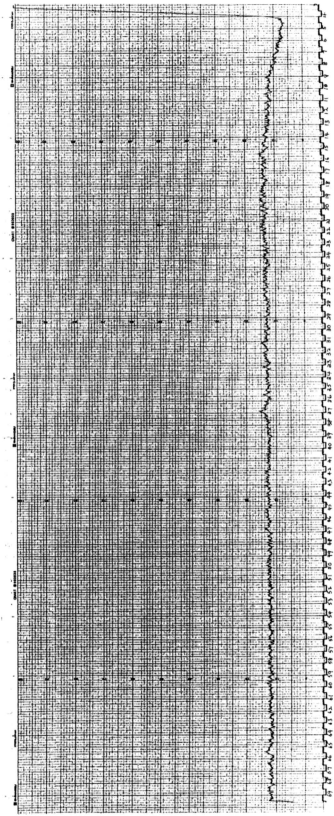

Figure 4.13 : X-ray diffractogram for sample F400

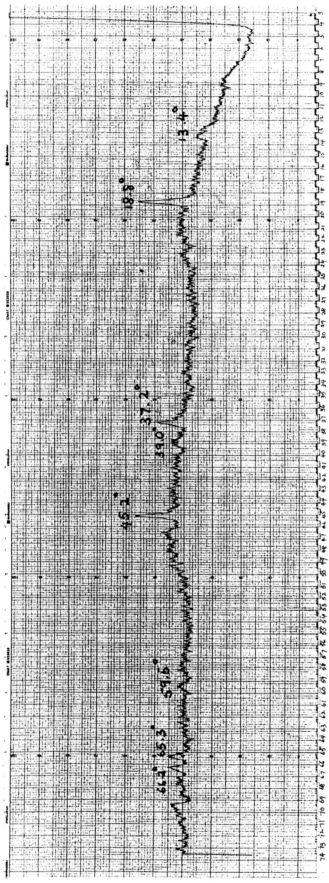

Figure 4.14 : X-ray diffractogram for sample F800

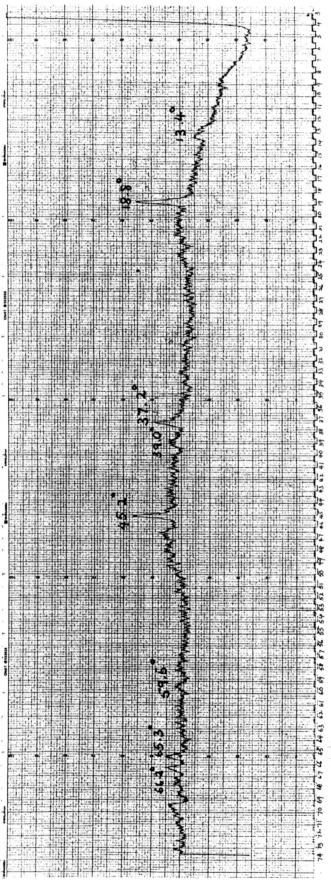

Figure 4.14 : X-ray diffractogram for sample F800

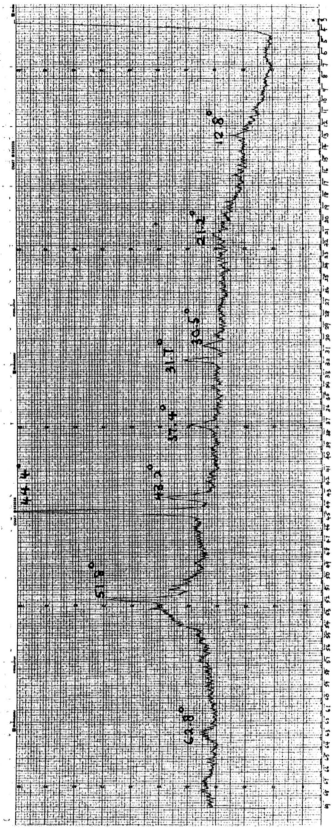

Figure 4.15 : X-ray diffractogram for sample E400

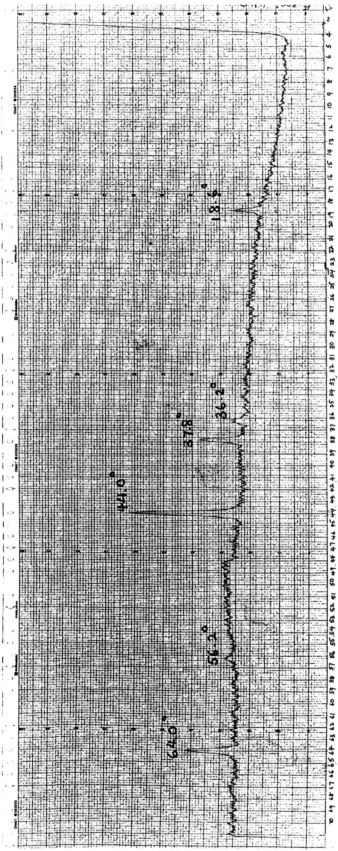

Figure 4.16 : X-ray diffractogram for sample E800

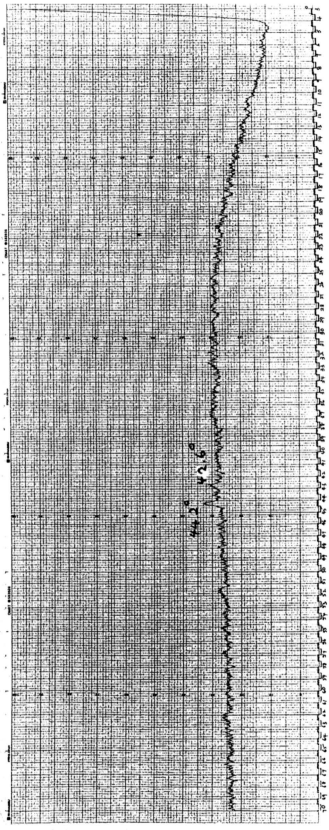

Figure 4.17 : X-ray diffractogram for sample A400

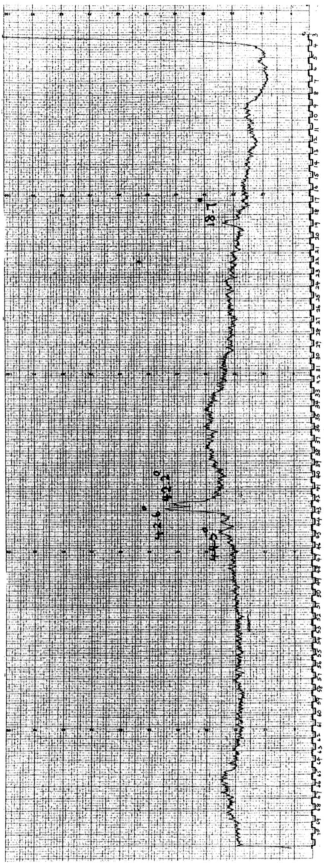

Figure 4.18 : X-ray diffractogram for sample A800

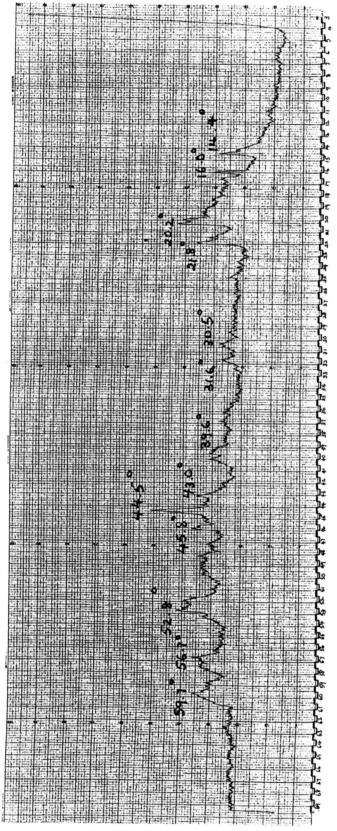

Figure 4.19 : X-ray diffractogram for sample C400

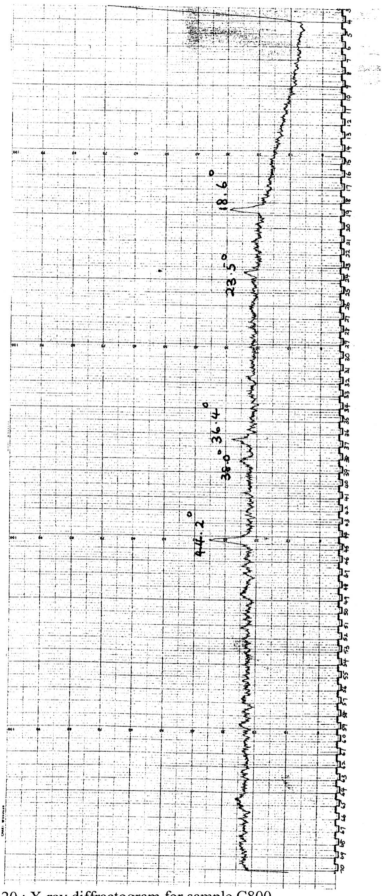

Figure 4.20 : X-ray diffractogram for sample C800

4.3 Cyclic Voltammetry

Cyclic voltammetry is perhaps the most effective and versatile electroanalytical technique available for mechanistic study of redox systems (Heinemann and Kissinger, 1996). It enables the electrode potential to be scanned rapidly in search of redox couples. Cyclic voltammetry was carried out on samples A, C, E and F, which were calcined for 400°C and 800°C for five hours. A scan rate of 400 mVs^{-1} and 100 mVs^{-1} were used.

Sample F

The cyclic voltammogram F400 at scan rate 400 mVs^{-1} clearly shows one redox loop

Possible reaction mechanism:

$Co^{II} - Co^{II} + e \rightleftharpoons Co^{I} - Co^{II}$ electron transfer

$Co^{I} - Co^{II} + Li^{+} \rightleftharpoons Co^{II} - Li - Co^{II}$ lithium ion diffusion

For scan rate of 100mVs^{-1}, there were two staircase increase in currents observed at +1V and +2V versus Ag/AgCl. This could be due redox reaction of Co(II) and Co(I).

$Co(II) + e \rightleftharpoons Co(I)$ electron transfer

$Co(I) + e \rightleftharpoons Co$ electron transfer

The cyclic voltammogram for sample F800 carried out at scan rate 100 mVs^{-1}, shows three redox loops. This shows, that cobalt most likely exist in more than one oxidation state at higher calcination temperature. It can be attributed to the formation of $LiCoO_2$, which is in agreement with X-ray diffraction pattern.

Possible reaction mechanism:

1) $Co^{II} - Co^{II} + e \rightleftharpoons Co^{I} - Co^{II}$ electron transfer

$Co^{I} - Co^{II} + Li^{+} \rightleftharpoons Co^{II} - Li - Co^{II}$ lithium ion diffusion

2) $Co^{III} - Co^{III} + e \rightleftharpoons Co^{II} - Co^{III}$ electron transfer

$Co^{II} - Co^{III} + Li^{+} \rightleftharpoons Co^{III} - Li - Co^{III}$ lithium ion diffusion

3) $Co^{II} - Co^{III} + e \rightleftharpoons Co^{II} - Co^{II}$ electron transfer

$Co^{II} - Co^{III} + Li^{+} \rightleftharpoons Co^{III} - Li - Co^{III}$ lithium ion diffusion

For both F800 and F400, the redox current was the same at scan rate for 400 mVs^{-1} and 100 mVs^{-1}.

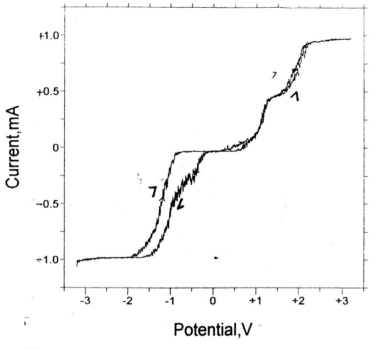

Scan rate $100mVs^{-1}$

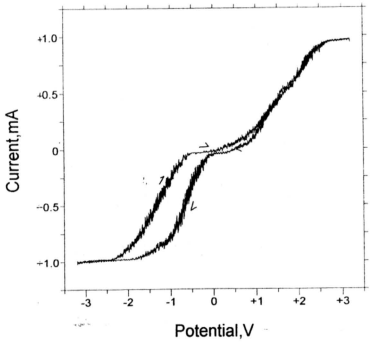

Scan rate $400mVs^{-1}$

Figure 4.21: Voltammogram for F400 at 26°C.

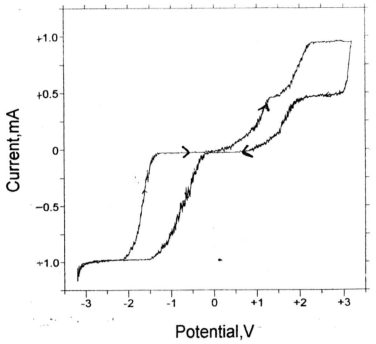

Scan rate 100mVs^{-1}

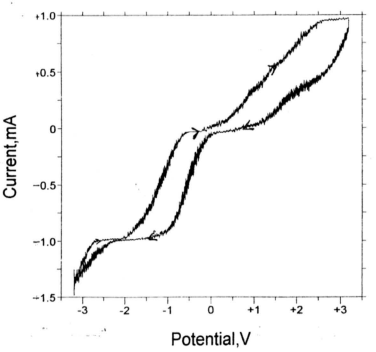

Scan rate 400mVs^{-1}

Figure 4.22: Voltammogram for F800 at 26°C.

Sample E

For sample E heated at 400°C, there is only one redox loop at scan rate $400mVs^{-1}$. This could be attributed, to the present of only one species of nickel, which is Ni (II)

Possible reaction mechanism:

$Ni^{II} - Ni^{II} + e \rightleftharpoons Ni^{II} - N^{I}$ electron tranfer

$Ni^{II} - Ni^{I} + Li^{+} \rightleftharpoons Ni^{II} - Li - Ni^{II}$ lithium ion diffusion

Cyclic voltammogram for E800 at $100mVs^{-1}$ clearly shows at least four redox loops. The heating of precursor sample at 800°C has probably converted most of the nickel, from Ni(II) to Ni (III). X-ray diffraction pattern, confirms the formation of crystalline $LiNiO_2$.

Possible reaction mechanism :

1) $Ni^{II} - Ni^{II} + e \rightleftharpoons Ni^{I} - Ni^{II}$ electron transfer

$Ni^{I} - Ni^{II} + Li^{+} \rightleftharpoons Ni^{II} - Li - Ni^{II}$ lithium ion diffusion

2) $Ni^{III} - Ni^{III} + e \rightleftharpoons Ni^{II} - Ni^{III}$ electron transfer

$Ni^{II} - Ni^{III} + Li^{+} \rightleftharpoons Ni^{III} - Li - Ni^{III}$ lithium ion diffusion

3) $Ni^{II} - Ni^{III} + e \rightleftharpoons Ni^{II} - Ni^{II}$ electron transfer

$Ni^{II} - Ni^{II} + Li^{+} \rightleftharpoons Ni^{II} - Li - Ni^{III}$ lithium ion diffusion

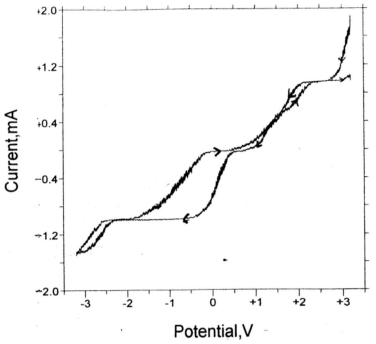

Scan rate 100 mVs^{-1}

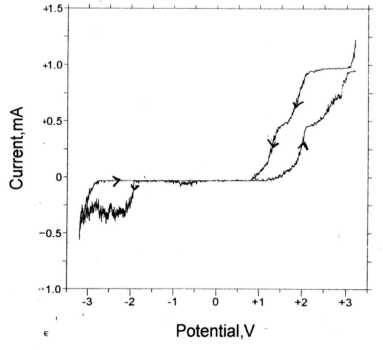

Scan rate 400mVs^{-1}

Figure 4.23 : Voltammogram for E400 at 26^{o}C

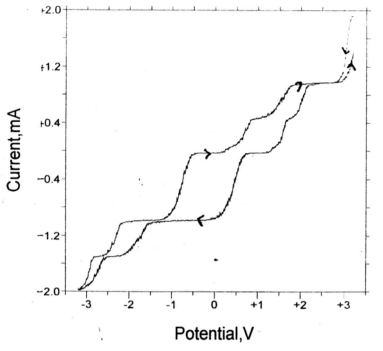

Scan rate 100 mVs^{-1}

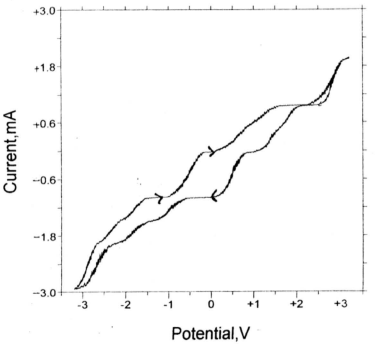

Scan rate 400mVs^{-1}

Figure 4.24 : Voltammogram for E800 at 26°C

Sample A

Cyclic voltammetery at a scan rate of $100mVs^{-1}$ for sample A calcined at 400oC showed at least three redox loops

Possible reaction mechanism:

1) $Co^{II} - Co^{II} + e \rightleftharpoons Co^{I} - Co^{II}$ electron transfer

$Co^{I} - Co^{II} + Li^{+} \rightleftharpoons Co^{II} - Li - Co^{II}$ lithium ion diffusion

2) $NI^{II} - Ni^{II} + e \rightleftharpoons Ni^{I} - Ni^{II}$ electron transfer

$Ni^{I} - Ni^{II} + Li^{+} \rightleftharpoons Ni^{II} - Li - Ni^{II}$ lithium ion diffusion

3) $Co^{II} - Ni^{II} + e \rightleftharpoons Co^{I} - Ni^{II}$ electron transfer

$Co^{I} - Ni^{II} + Li^{+} \rightleftharpoons Co^{II} - Li - Ni^{II}$ lithium ion diffusion

4) $Co^{II} - Ni^{II} + e \rightleftharpoons Co^{II} - Ni^{I}$ electron transfer

$Co^{II} - Ni^{I} + Li^{+} \rightleftharpoons Co^{II} - Li - Ni^{II}$ lithium ion diffusion

Sample A calcined at 800°C showed least two redox loops at a scan rate of $100mVs^{-1}$. There was not much difference between A400 and A800.

The redox currents were the same for both scan rates.

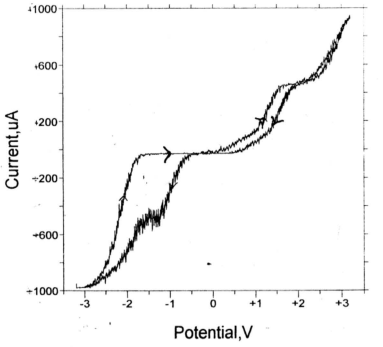

Scan rate $100mVs^{-1}$

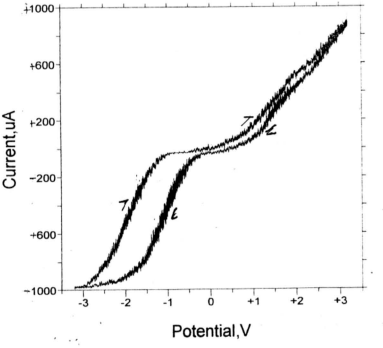

Scan rate $400mVs^{-1}$

Figure 4.25 : Voltammogram for A400 at 26°C

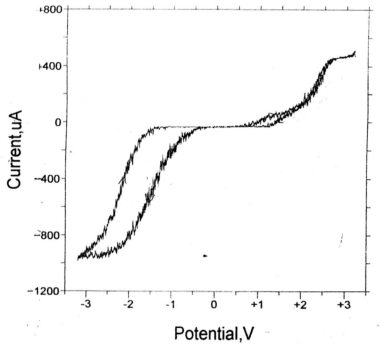

Scan rate 100mVs $^{-1}$

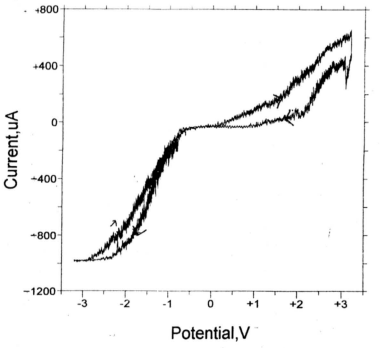

Scan rate 400mVs^{-1}

Figure 4.26: Voltammogram for A800 at 26^{o}C.

Sample C

For sample C, calcined at 400°C and 800°C, the cyclic voltammogram showed at least two redox loops. The redox loops can be attributed to any of the two reactions described for A400 and A800. It was also noticed that the redox current was the same for scan rate at $100mVs^{-1}$ and $400mVs^{-1}$

Cyclic voltammetry was carried at 60°C at a scan rate of $100mVs^{-1}$ for sample A800, C800, F800. The voltammogram for these samples, shown in figures 4.29 - 4.32 show more redox loops than for experiment carried out at 26°C. A possible explanation for this phenomenon, is that lithium ion can intercalate at different sites. More work has to be done at higher temperatures and using materials with different crystalline structure (e.g. $LiMn_2O_4$) to confirm the above suggestion.

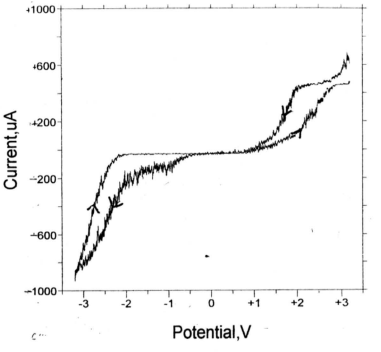

Scan rate $100mVs^{-1}$

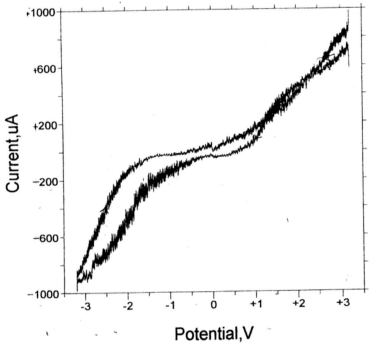

Scan rate $400mVs^{-1}$

Fig 4.27: Voltammogram for C400 at 26°C

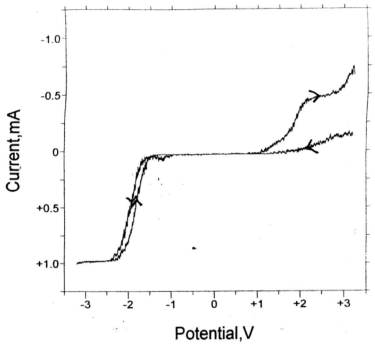

Scan rate $100mVs^{-1}$

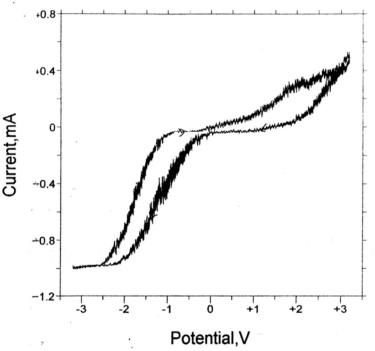

Scan rate $400mVs^{-1}$

Figure 4.28 : Voltammogram for C800 at 26°C.

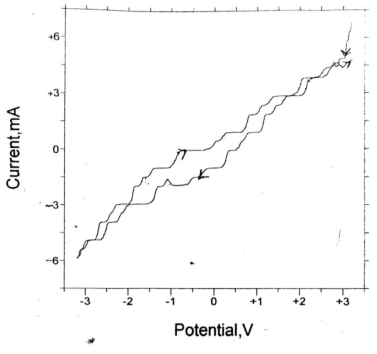

Figure 4.29: Voltammogram for F800 at 60°C

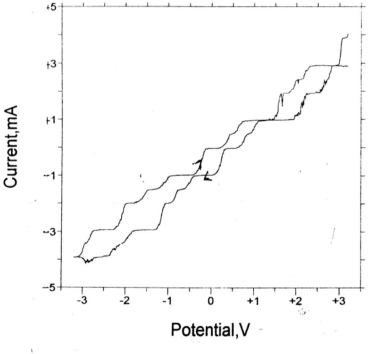

Figure 4.30: Voltammogram for E800 at 60°C

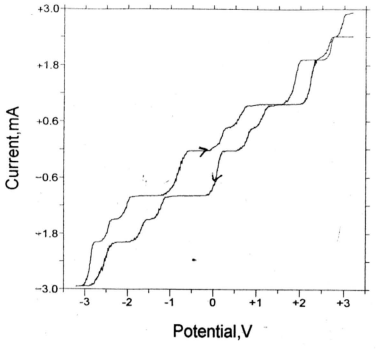

Figure 4.31: Voltammogram for A800 at 60°C

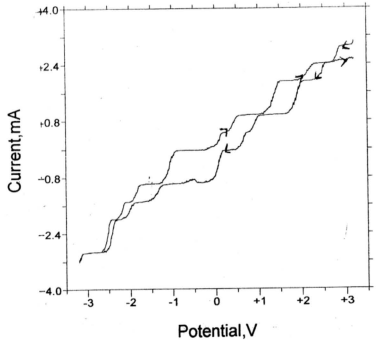

Figure 4.32: Voltammogram for C800 at 60°C

From cyclic voltammogram the current remained the same at scan rate of $100mVs^{-1}$ and $400mVs^{-1}$. In other words, the current was not dependent on the scan rate, i.e., 'I is not proportional to $v^{1/2}$ '.Therefore, the redox couples were not diffusion controlled, so, the diffusion of lithium ion along the lithium oxide is not the rate determining step. Resistance of samples A, C, E and F calcined at different temperatures have been measured and values are in the range of few hundred kilo ohms to few mega ohms. The resistance is higher than that of semiconductor materials. Since the resistances of these materials are quite high, the rate-determining step is the electron transfer in the lithium transition metal oxide.

4.4 Battery Performance

The assembled cell C/electrolyte/$LiNiO_2$ was cycled galvanostatically for charge/discharge characteristics. Since the cell in the assembled mode is dead, the cell has to be charged. The cell was charged at a constant current of 1.0mA for 1 minute and discharged at a constant current of 0.1mA for 1 minute. The cell was cycled between the range 4V and 0V. Figure 4.33 and figure 4.34 show the charge-discharge curve for cell using $LiNiO_2$ as the active cathode materials. It can be inferred that lithium ions could have deintercalated $LiNiO_2$ entered the electrolyte and intercalated with the carbon anode. When discharged, the lithium ion would de-intercalate from the anode and migrates back to the cathode material.

$LiNiO_2 \longrightarrow Li_{1-x}NiO_2 + xLi^+ + xe$ [cathode reaction]

$C_6 + xLi \longrightarrow Li_xC_6$ [anode reaction]

$C_6 + LiNiO_2 \longrightarrow Li_xC_6 + Li_{1-x}NiO_2$ [0<X>1]

The poor performance of the battery could be attributed to high resistance, polarization and bad fabrication but does provide evidence of intercalation and deintercalation of Li^+ in the material prepared and so does not defeat the purpose or objective of the project.

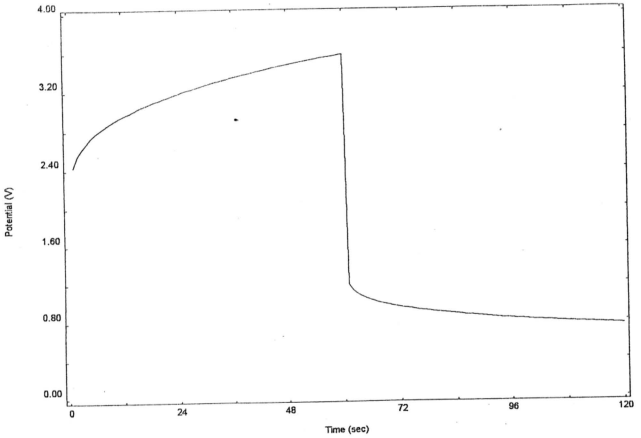

Figure 4.33 : Charge/discharge cycle for $LiNiO_2$ (1^{st} Cycle)

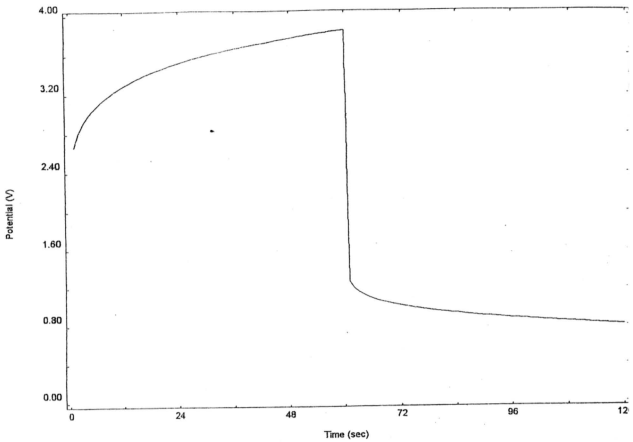

Figure 4.34 : Charge/discharge cycle for $LiNiO_2$ (2^{nd} cycle)